

The properties of prompt emission in short GRBs with extended emission observed by *Fermi*/GBM

Lin Lan¹, Rui-Jing Lu¹, Hou-Jun Lü^{1*}, Jun Shen¹, Jared Rice², Long Li¹, and En-Wei Liang

¹*Guangxi Key Laboratory for Relativistic Astrophysics, School of Physical Science and Technology, Guangxi University, Nanning 530004, China*

²*Department of Physics, Texas State University, San Marcos, TX 78666, USA*

13 March 2024

ABSTRACT

Short GRBs with extended emission (EE) that are composed initially of a short-hard spike and followed by a long-lasting EE, are thought to be classified as a subsection of short GRBs. The narrow energy band available during the *Swift* era combined with a lack of spectral information prevented discovery of the intrinsic properties of those events. In this paper, we performed a systematic search of short GRBs with EE by using all available *Fermi*/GBM data. The search identified 26 GBM-detected short GRBs with EE that are similar to GRB 060614 observed by *Swift*/BAT. We focus on investigating the spectral and temporal properties for both the hard spike and the EE components of all 26 GRBs, and explore differences and possible correlations between them. We find that while the peak energy (E_p) of the hard spikes is a little bit harder than that of the EE, but their fluences are comparable. The harder E_p seems to correspond to a larger fluence and peak flux with a large scatter for both the hard spike and EE components. Moreover, the E_p of both the hard spikes and EE are compared to other short GRBs. Finally, we also compare the properties of GRB 170817A with those short GRBs with EE and find no significant statistical differences between them. We find that GRB 170817A has the lowest E_p , likely because it was off-axis.

Key words: gamma-ray burst: general- methods: statistical

1 INTRODUCTION

Phenomenologically, gamma-ray bursts (GRBs) have been generally divided into “long soft” and “short hard” classes based on the observed bimodal distribution in duration and hardness ratio (Kouveliotou et al. 1993). The progenitors of long GRBs likely originate from the core collapse of a massive star, e.g. via observations of associated supernovae (Narayan et al. 1992; Woosley 1993; Galama et al. 1998; Hjorth et al. 2003; Stanek et al. 2003; Woosley & Bloom 2006), and the progenitors of short GRBs are likely the coalescence of two compact objects, i.e. neutron star - neutron star (NS-NS) or neutron star - black hole (NS-BH) systems (Paczynski 1986; 1991 Eichler et al. 1989).

Within the short GRB class, there is a subsection of bursts that is characterized by a short/hard spike (with a duration ~ 5 s) followed by a series of soft gamma-ray pulses with a much longer duration (called extended emission; Norris & Bonnell 2006; Troja et al. 2008; Perley et al. 2009). Since the discovery of the first clear evidence of extended

emission (EE) in GRB 060614 (Gehrels et al. 2006; Gal-Yam et al. 2006; Fynbo et al. 2006; Della Valle et al. 2006), there has been an extensive search for more of these types of events are in both the *Swift* (Zhang et al. 2009; Norris et al. 2010; Sakamoto et al. 2011) and *Fermi* eras (Kaneko et al. 2015).

From the theoretical point of view, a number of different models have been proposed to interpret short GRBs with EE. For instance, the EE could be the product of an accretion disc around a magnetar undergoing magnetic propeller-ing (Metzger et al. 2008; see also Zhang & Dai 2008, 2009; Piro & Ott 2011; Gompertz et al. 2013; Bernardini et al. 2014; Gibson et al. 2017), the magnetic dipole spin-down of a magnetar (Dai & Lu 1998a,b; Zhang & Mészáros 2001; Fan & Xu 2006; Bucciantini et al. 2012; Rowlinson et al. 2013; Lü et al. 2015), a two-jet solution (Barkov & Pozanenko 2011), r-process heating of the accretion disc (Metzger et al. 2010), or magnetic reconnection and turbulence (Zhang & Yan 2011). Liu et al. (2012) suggested that the short GRBs with EE may arise from radial angular momentum transfer in the disk and the magnetic barrier around the black hole. Lü et al. (2015) proposed that EE components detected in

* E-mail: lhj@gxu.edu.cn

the BAT band could be simply the internal plateau emission when that emission is bright and hard enough. In any case, the rapid variability of this EE strongly suggests that it results from ongoing central engine activity (Perley et al. 2009; Metzger et al. 2011).

The central engine and radiation mechanism of short GRBs with EE remain open questions, but the intrinsic spectra of both the hard spike and EE components may provide some important clues for understanding these questions. In the *Swift* era, some systematic analyses of the spectral properties of short GRBs with EE show that the EE component is softer than the hard spike (Villasenor et al. 2005; Norris & Bonnell 2006; Troja et al. 2008; Perley et al. 2009). However, the spectra of both the initial hard spike and subsequent EE components are well-fitted by a power-law model, which can not reflect the intrinsic properties of the spectra. Kaneko et al. (2015) performed a systematic comparison of the short GRBs with EE observed by *Swift*/BAT with those observed by *Fermi*/GBM. However, they only considered the NaI detectors of GBM in their spectral analysis and ignored the contributions from the BGO detectors. This may be the reason why most of the short GRBs with EE can be fitted with a power-law model in Kaneko et al. (2015).

More interestingly, the short GRB 170817A associated with the gravitational wave event (GW 170817) from double a NS merger was recently detected by *Fermi*/GBM (Abbott et al. 2017; Goldstein et al. 2017), and was found to have a prompt emission that is composed of a hard spike of 0.8 s and a weak tail of up to 2.3 s (Goldstein et al. 2017; Zhang et al. 2018; Pozanenko et al. 2018). An interesting question is whether or not GRB 170817A differs in its spectral properties from other typical short GRBs with EE.

Although the short GRBs with EE have been investigated from both statistical and theoretical analyses, it remains unclear whether the initial hard spike differs in spectral properties from the subsequent EE component. What are the relationships between the hard spike and subsequent EE component? Do the hard spike and subsequent EE component share the same physical origin? The aim of this paper is to address these interesting questions through a systematic analysis of the *Fermi*/GBM data by considering the contribution of the high-energy detector. Our data reduction and sample selection are presented in §2. Some comparisons between the hard spike and subsequent EE component for our sample, as well as other typical short GRBs and GRB 170817A, are reported in §3. The conclusions and discussion are drawn in §4.

2 DATA REDUCTION AND SAMPLE SELECTION

The *Fermi* satellite has operated for more than ten years, and provides unprecedented spectral coverage over seven orders of magnitude in energy (from ~ 8 keV to ~ 300 GeV). There are two instruments onboard the *Fermi* satellite. One is the Gamma-ray Burst Monitor (GBM; Meegan et al. 2009), which has twelve sodium iodide (NaI) and two bismuth germanate (BGO) scintillation detectors covering an energy band from 8 keV to 40 MeV. There are three types of data modes CTIME, CSPEC, and TTE, which correspond

to a time resolution of 64 ms, 1.024 s, and any bin size, respectively (Paciesas et al. 2012). We select only the TTE data in our analysis due to including individual photons arriving with time and energy tags¹, and any time resolution bin size can be selected to perform the spectral and temporal analysis. The other instrument onboard *Fermi* is the Large Area Telescope (LAT) with an energy coverage from 20 MeV to 300 GeV (Atwood et al. 2009). Here, we consider only GBM data for the temporal and spectral analysis and ignore the contributions of LAT data because the physical origin of high-energy photons remain an open question (e.g., originating from internal or external dissipation).

2.1 Lightcurve extraction

We obtain the original GBM data (from the twelve NaI and two BGO detectors) from the public science support center at the official *Fermi* web site². We select the brightest detector in NaI and BGO for our analysis because the brightest detector has the minimum angle between the incident photon and the normal direction of the detector. Based on the standard *heasoft* tools (version 6.19) and the *Fermi ScienceTools* (v10r0p5), we developed a *Python* code to extract the energy-dependent lightcurves and time-dependent spectra using the spectral source package *gtBurst*³. For more details of lightcurve extraction with the Bayesian Block algorithm, please refer to our latest paper Lan et al. (2018). Moreover, we calculated the duration of both the hard spike ($T_{d,s}$) and subsequent EE ($T_{d,e}$), which are reported in Table 1.

2.2 Sample selection criteria

As of December 2018, we have extracted the lightcurves of more than 2400 GRBs which were detected by *Fermi*/GBM. GRB 060614 was the first clear case of a short GRB with EE; its lightcurve of prompt emission is composed of a short spike with ~ 5 s and followed a longer soft emission (Gehrels et al. 2006; Gal-Yam et al. 2006; Fynbo et al. 2006; Della Valle et al. 2006). We adopt the properties of the lightcurve of GRB 060614 as the “standard event” to search for in our samples, with the following three criteria:

- (i) The duration of the initial hard spike is less than 5 seconds, and is followed by a longer soft emission lasting a few seconds to hundreds of seconds.
- (ii) The signal-to-noise ratio (S/N) of the initial spike and EE components should be greater than 3σ .
- (iii) The count rates remain below 30%–40% of the peak count rate for at least 50% of the rest of the duration after the peak time until $T_0 + 5$ s (see also Kaneko et al. 2015).

There are 26 GRBs that satisfy with our criteria up to December 2018. No redshifts are measured in our sample. A comparison of our sample with that of Kaneko et al. (2015) shows only four overlapping GRBs, which may be due to different sample selection criteria. An example lightcurve

¹ CTIME and CSPEC data are not used in our analysis due to the fixed time resolution of 64 ms and 1.024 s, respectively.

² <http://fermi.gsfc.nasa.gov/ssc/data/>.

³ <http://sourceforge.net/projects/gtbust/>.

from our sample is the GRB 161218B lightcurve shown in Figure 1.

2.3 Spectrum Extraction and fitting

We select two time intervals that are long before and far after the prompt emission as the background, and subtract it from the burst phase using a polynomial function fit. Then, XSPEC is used to perform time-integrated spectral fits for the initial hard spike, subsequent EE, as well as the entire burst (see Figure 1). In order to determine evolutionary behavior during the prompt emission phase, the time-resolved spectra are also required (see Figure 1). The statistic χ^2 is adopted to judge the goodness of the spectral fits. Moreover, the energy channels in the vicinity of the iodine K-edge at 33.17 keV were excluded to better assess the quality of the fit of the spectral models (Goldstein et al. 2012).

A Band function model is the prevailing model for doing the spectral fit (Band et al. 1993). Alternatively, a cutoff power-law (CPL) or simple power-law (PL) model can be fit if the Band function model is not a good enough fit to the data. They can be written as

$$N_{\text{CPL}}(E) = A \cdot E^{-\alpha} \exp\left(-\frac{E}{E_p}\right), \quad (1)$$

$$N_{\text{PL}}(E) = A \cdot E^{-\alpha}, \quad (2)$$

where A is the normalization of the spectrum, and α and E_p are the low-energy photon spectral index and peak energy, respectively. On the other hand, we also attempt to take into account a black body (BB) model or multi-component superposition models (e.g., BB+Band, BB+CPL, and BB+PL) to fit the spectra of both the initial spike and EE, but they do not significantly improve the goodness and they contain more free parameters compared to the CPL model. Thus the CPL model is the optimal selection for both the hard spike and EE in our sample, except the hard spike component of GRB 081215 (bn081215784) that can be fit with a Band function. An example of spectral fitting in our sample is shown in Figure 1, and the spectral parameters derived from our fits are reported in Table 1.

3 RESULTS

3.1 Statistical comparisons with the hard spike and EE

As early as the Compton Gamma-Ray Observatory (CGRO) era, Ford et al. (1995) first found there are two different E_p -evolution patterns (i.e., hard-to-soft and intensity tracking) in the prompt emission phase of long GRBs by performing a comprehensive analysis of Burst And Transient Source Experiment (BATSE) data. After that, it was revisited by many other authors who obtained similar results with those in Ford et al. (1995) (e.g., Liang & Kargatis 1996; Boronovo & Ryde 2001; Kaneko et al. 2006; Lu et al. 2012). Here, we also analyze the time-resolved spectrum of both the hard

spike and subsequent EE for twenty GRBs of our sample⁴. We find that the E_p -evolution of five GRBs in our sample follow the hard-to-soft pattern, twelve GRBs have intensity tracking, and the E_p of three GRBs does not evolve significantly. We also derive the bolometric fluence in the 8 keV – 40 MeV band for both the hard spike ($S_{\gamma,s}$) and EE ($S_{\gamma,e}$), as well as the peak flux. Moreover, we compare the peak energy of the hard spike ($E_{p,s}$) with that of the EE component ($E_{p,e}$) by analyzing time-integrated spectral fits.

Figure 2(a) shows the correlation of peak energy between the hard spike and subsequent EE. We find that the peak energy of the hard spikes in our sample is higher than the peak energy of the EE. This result is roughly consistent with results from the *Swift* and *Fermi* eras (Norris & Bonnell 2006; Kaneko et al. 2015). However for GRB 090831A, the peak energy of its EE component is higher than that of its initial hard spike. In order to test whether the peak energy value of the EE component of this case is valid, we compare the spectral fitting models. We invoke the Bayesian information criterion (BIC)⁵, which is an evaluation criterion for models defined by considering both the free parameters of the model and the goodness of the fit (Lü et al. 2017). We find the $\Delta\text{BIC} \gg 10$, which means the CPL model is strongly preferred, and the measured peak energy of EE component of GRB 090831A is valid.

Figure 2(b) presents the distribution of peak energy for the hard spike and subsequent EE. The E_p distributions range from tens of keV to one thousand keV. Both follow lognormal distributions with peaks at $E_{p,s} = (447 \pm 78)$ keV and $E_{p,e} = (282 \pm 57)$ keV, respectively. We measure the difference of any pair of distributions with the probability P_{KS} given by the Kolmogorov–Smirnov (KS) test, as proposed by Ashman et al. (1994). The hypothesis that the two distributions are from the same parent sample is statistically rejected if $P_{\text{KS}} < 10^{-4}$, and it is marginally rejected if $10^{-4} < P_{\text{KS}} < 0.1$. A probability $P_{\text{KS}} = 1$ indicates that the two samples are identical. The KS test on our sample returned a probability $P_{\text{KS}} = 0.11$, which indicates that the two peak energy distributions are marginally similar, but are likely different. On the other hand, the minor differences between the distributions may be not caused from the physically, but due to a selection effect.

Similarly, Figure 2(c) and (d) show the correlation and distribution of fluence for the hard spike and subsequent EE. The fluence distributions of the hard spike and EE

⁴ There are 26 short GRBs with EE in our sample, but only 20 GRBs that have enough photons for an analysis of the time-resolved spectrum.

⁵ BIC is a criterion for model selection among a finite set of models. The model with the lowest BIC is preferred. BIC can be expressed as: $\text{BIC} = \chi^2 + k \cdot \ln(n)$, where k is the number of model parameters and n is the number of data points. The strength of the evidence against the model with the higher BIC value can be summarized as follows:

- (1) if $0 < \Delta\text{BIC} < 2$, the evidence against the model with higher BIC is weak;
- (2) if $2 < \Delta\text{BIC} < 6$, the evidence against the model with higher BIC is positive;
- (3) if $6 < \Delta\text{BIC} < 10$, the evidence against the model with higher BIC is strong;
- (4) if $10 < \Delta\text{BIC}$, the evidence against the model with higher BIC is very strong.

are also lognormal with mean values of $\log S_{\gamma,s} = (-5.11 \pm 0.04)$ erg cm⁻² and $\log S_{\gamma,e} = (-5.08 \pm 0.10)$ erg cm⁻², respectively. The KS test on these two distributions returned a probability $P_{KS} = 0.44$, which indicates that they cannot be absolutely distinguished.

In the CGRO era, a hardness-intensity correlation was discovered in the GRB prompt emission phase in an analysis of BATSE data (Dezalay et al. 1998; Borgonovo & Ryde 2001). Figure 3 presents the correlations of $E_p - F_p$, $E_p - S_\gamma$, $S_\gamma - F_p$, and $F_p - T_d$ of the hard spike and EE for the entire sample. It seems to be that a higher peak flux or fluence generally has a higher peak energy, but there is no significant correlation between the peak flux and the duration of the hard spike and EE.

One basic question is what is the difference between the estimated fluence in our calculation of EE versus hard spike with that of Kaneko et al. (2015)? Figure 4 shows the comparison of the fluences between the two phases for four overlapping GRBs in the two samples. We find that the fluence of both the hard spike and EE components in our calculation is larger than that of Kaneko et al. (2015). Several factors may explain such a difference, e.g. the selection of different energy bands used in calculating the fluence⁶, the use of a non-standard definition of duration (5 seconds versus 2 seconds for T_{90}), or different spectral fitting models.

3.2 Short GRBs with EE vs. other typical short GRBs

Troja et al. (2008) proposed that the short GRBs with EE and typical short GRBs may originate from different progenitors (i.e., NS-BH or NS-NS mergers) by comparing the offsets from their host galaxies. If this is the case, the different progenitors may correspond to different observational properties. In this section, we compare the temporal and spectral properties between the short GRBs with EE and other typical short GRBs in the *Fermi* era. Moreover, we also determine if there is a difference between the hard spike and EE components in our sample compared to other typical short GRBs.

Lu et al. (2017) presented a comprehensive analysis of short GRBs observed with *Fermi*/GBM and derived a catalog of 275 typical short GRBs, which contains a peak energy distribution across a wider range of tens to thousands of keV. We compared our sample to their more extensive catalog. In Figure 5 we make some comparisons. The top three panels present the $E_p - \text{Flux}$, $E_p - T_d$, and $\text{Flux} - T_d$ diagrams. The E_p is measured via time-integrated spectral fits from the beginning of the spike to end of the EE, and Flux and T_d are the average flux and duration of the burst, respectively. Both E_p and Flux are not significantly different when comparing the short GRBs with EE with other typical short GRBs.

Moreover, it is necessary to test whether the hard spike and subsequent EE components are different in comparison to other typical short GRBs. We separate the hard spike component and EE component to measure their E_p , flux,

and T_d values. The bottom three panels of Figure 5 show the comparisons of E_p , flux, as well as T_d for the hard spike, EE, and other short GRBs. The distribution of E_p for other typical short GRBs is in a wider range. We find that the E_p of hard spike in our sample is tended to a higher E_p side of other short GRBs, but EE component is tended to a lower E_p side of other short GRBs. However, from the statistical point of view, the E_p distributions of hard spike and EE components are not significant distinction with other typical short GRBs, this may be caused by selection effects. Figure 6 presents the distributions of E_p of SGRBs, SGRBs with EE (hard spike), and SGRBs with EE (time-integrated). We find that they follow log-normal distributions with peaks at $E_{p,s} = (302 \pm 22)$ keV (SGRBs), $E_{p,s} = (380 \pm 77)$ keV (SGRBs with EE), and $E_{p,s} = (447 \pm 78)$ keV (hard spikes). There are minor differences between them, but nothing significant. From a statistical point of view, these small differences may be due to the number of sources we used in our statistical analysis. Those results suggest that one can not distinguish the progenitors of short GRBs with EE and other typical short GRBs via their spectral properties alone.

3.3 GRB 170817A in comparison to short GRBs with EE

GRB 170817A is a short GRBs associated with the gravitational wave event (GW170817) from the double NS merger which was recently detected by *Fermi*/GBM (Abbott et al. 2017; Goldstein et al. 2017). An analysis of the prompt emission of GRB 170817A shows that it consists of two different components. The first component is a short hard spike whose spectrum can be fit by a CPL with peak energy $E_p = 230^{+310}_{-80}$ keV. The preferred fit for the spectrum of the second component is a blackbody model with $kT = 11.3^{+3.8}_{-2.4}$ keV (Goldstein et al. 2017; Zhang et al. 2018), but a non-thermal origin with a CPL model fit of $E_p = 43^{+9}_{-7}$ keV cannot be ruled out (Zhang et al. 2018; Pozanenko et al. 2018). In this section, we compare the properties of GRB 170817A to the short GRBs with EE in our sample.

Based on Figures 2 and 3, we find that the peak energy and fluence of the EE, and the fluence of the hard spike for GRB 170817A are the lowest in comparison to all of our samples, but the peak energy of the hard spike for GRB 170817A is not the lowest. Moreover, the peak flux of both the hard spike and EE of GRB 170817A are smallest out of all our samples. The possible reason may be that GRB 170817A is an off-axis observation (Abbott et al. 2017; Alexander et al. 2018; Biehl et al. 2018; Ioka & Nakamura 2019).

4 CONCLUSIONS

We have presented a comprehensive temporal and spectral analysis for the GRB data observed with *Fermi*/GBM during nine years of operation. By adopting the criterion of GRB 060614, we find that a small fraction of GRBs observed by *Fermi*/GBM are similar to GRB 060614. The prompt emission light curves of those events exhibit a hard spike initially and followed a soft tail emission, so called short GRBs with extended emission. We try to determine the differences between the initial hard spike and EE components of our sample, as well as the differences between short GRBs with

⁶ The fluence in Kaneko et al. (2015) is calculated in the energy range 15-350 keV, while we used the energy band 8-1000 keV to estimate the fluence.

EE and other typical short GRBs observed by *Fermi*/GBM. Our results are summarized as follows:

- We obtained a sample of 26 short GRBs with EE that were observed with *Fermi*/GBM. The peak energy of both the initial hard spike and subsequent EE component can be estimated via spectral fits with a CPL model or a Band model.

- The peak energy of the EE components in our sample seems to be softer a little bit than the peak energy of the initial hard spike episodes, except for GRB 090831A, but the total fluence of the hard spike and subsequent EE are comparable with each other. Moreover, it seems to be that a higher peak flux or fluence generally has a higher peak energy for both the hard spikes and EE, but we do not find a significant correlation between peak flux and the duration of the hard spike and EE.

- Both the peak energy and average flux of short GRBs with EE in our sample are not significantly different in comparison to other short GRBs observed by *Fermi*/GBM. Moreover, the properties of the hard spike and followed EE components are also not significantly distinct in comparison with other short GRBs. These results suggest that the short GRBs with EE in our sample likely share a similar physical origin.

Moreover, the distribution of E_p for other typical short GRBs is in a wider range, and the E_p of hard spike in our sample is tended to a higher E_p side of other short GRBs, but EE component is tended to a lower E_p side of other short GRBs. However, from the statistical point of view, the E_p distributions of hard spike and EE components are not significant distinction with other typical short GRBs, this may be caused by selection effects and sample selection criteria. On the other hand, the distribution of E_p of SGRBs with EE (time-integrated) is between the that of SGRBs with EE (hard spike) and typical short SGRBs. The minor differences between them seem to not be from the physically, but likely to be due to selection effects. Those results also suggest that one can not distinguish the progenitors of short GRBs with EE and other typical short GRBs via their spectral properties alone.

5 ACKNOWLEDGEMENTS

We acknowledge the use of the public data from the *Fermi* data archive. This work is supported by the National Natural Science Foundation of China (Grant Nos.11922301, 11603006, 11851304 and 11533003), the Guangxi Science Foundation (grant No. 2017GXNSFFA198008, AD17129006, and 2018GXNSFGA281007). The One-Hundred-Talents Program of Guangxi colleges, Bagui Young Scholars Program (LHJ), and special funding for Guangxi distinguished professors (Bagui Yingcai & Bagui Xuezhe).

REFERENCES

Abbott B. P., et al., 2017, *PhRvL*, 119, 161101
 Alexander K. D., et al., 2018, *ApJ*, 863, L18
 Ashman K. M., Bird C. M., Zepf S. E., 1994, *AJ*, 108, 2348
 Atwood W. B., et al., 2009, *ApJ*, 697, 1071
 Band D., et al., 1993, *ApJ*, 413, 281

Barkov M. V., Pozanenko A. S., 2011, *MNRAS*, 417, 2161
 Bernardini M. G., et al., 2014, *MNRAS*, 439, L80
 Bucciantini N., Metzger B. D., Thompson T. A., Quataert E., 2012, *MNRAS*, 419, 1537
 Biehl D., Heinze J., Winter W., 2018, *MNRAS*, 476, 1191
 Borgonovo L., Ryde F., 2001, *ApJ*, 548, 770
 Dai Z. G., Lu T., 1998a, *PhRvL*, 81, 4301
 Dai Z. G., Lu T., 1998b, *A&A*, 333, L87
 Della Valle M., et al., 2006, *Natur*, 444, 1050
 Dezalay J.-P., et al., 1998, *AIPC*, 428, 15
 Eichler D., Livio M., Piran T., Schramm D. N., 1989, *Natur*, 340, 126
 Fan Y.-Z., Xu D., 2006, *MNRAS*, 372, L19
 Ford L. A., et al., 1995, *ApJ*, 439, 307
 Fynbo J. P. U., et al., 2006, *Natur*, 444, 1047
 Gal-Yam A., et al., 2006, *Natur*, 444, 1053
 Galama T. J., et al., 1998, *Natur*, 395, 670
 Gehrels N., et al., 2006, *Natur*, 444, 1044
 Gibson S. L., Wynn G. A., Gompertz B. P., O'Brien P. T., 2017, *MNRAS*, 470, 4925
 Goldstein A., et al., 2017, *ApJ*, 848, L14
 Goldstein A., et al., 2012, *ApJS*, 199, 19
 Gompertz B. P., O'Brien P. T., Wynn G. A., Rowlinson A., 2013, *MNRAS*, 431, 1745
 Hjorth J., et al., 2003, *Natur*, 423, 847
 Ioka K., Nakamura T., 2019, *MNRAS*, 487, 4884
 Kaneko Y., Bostancı Z. F., Göğüş E., Lin L., 2015, *MNRAS*, 452, 824
 Kaneko Y., Preece R. D., Briggs M. S., Paciesas W. S., Meegan C. A., Band D. L., 2006, *ApJS*, 166, 298
 Kouveliotou C., Meegan C. A., Fishman G. J., Bhat N. P., Briggs M. S., Koshut T. M., Paciesas W. S., Pendleton G. N., 1993, *ApJ*, 413, L101
 Lü H.-J., et al., 2017, *ApJ*, 849, 71
 Lü H.-J., Zhang B., Lei W.-H., Li Y., Lasky P. D., 2015, *ApJ*, 805, 89
 Lü H.-J., Zhang B., Liang E.-W., Zhang B.-B., Sakamoto T., 2014, *MNRAS*, 442, 1922
 Lan L., et al., 2018, *ApJ*, 862, 155
 Liang E., Kargatis V., 1996, *Natur*, 381, 49
 Liu T., Liang E.-W., Gu W.-M., Hou S.-J., Lei W.-H., Lin L., Dai Z.-G., Zhang S.-N., 2012, *ApJ*, 760, 63
 Lu R.-J., Du S.-S., Cheng J.-G., Lü H.-J., Zhang H.-M., Lan L., Liang E.-W., 2017, *arXiv*, arXiv:1710.06979
 Lu R.-J., Wei J.-J., Liang E.-W., Zhang B.-B., Lü H.-J., Lü L.-Z., Lei W.-H., Zhang B., 2012, *ApJ*, 756, 112
 Meegan C., et al., 2009, *ApJ*, 702, 791
 Metzger B. D., Arcones A., Quataert E., Martínez-Pinedo G., 2010, *MNRAS*, 402, 2771
 Metzger B. D., Giannios D., Thompson T. A., Bucciantini N., Quataert E., 2011, *MNRAS*, 413, 2031
 Metzger B. D., Quataert E., Thompson T. A., 2008, *MNRAS*, 385, 1455
 Narayan R., Paczynski B., Piran T., 1992, *ApJ*, 395, L83
 Norris J. P., Bonnell J. T., 2006, *ApJ*, 643, 266
 Norris J. P., Gehrels N., Scargle J. D., 2010, *ApJ*, 717, 411
 Paciesas W. S., et al., 2012, *ApJS*, 199, 18
 Paczynski B., 1986, *ApJ*, 308, L43
 Paczynski B., 1991, *AcA*, 41, 257
 Perley D. A., et al., 2009, *ApJ*, 696, 1871
 Piro A. L., Ott C. D., 2011, *ApJ*, 736, 108
 Pozanenko A. S., et al., 2018, *ApJ*, 852, L30
 Rowlinson A., O'Brien P. T., Metzger B. D., Tanvir N. R., Levan A. J., 2013, *MNRAS*, 430, 1061
 Sakamoto T., et al., 2011, *ApJS*, 195, 2
 Stanek K. Z., et al., 2003, *ApJ*, 591, L17
 Troja E., King A. R., O'Brien P. T., Lyons N., Cusumano G., 2008, *MNRAS*, 385, L10

- Villasenor J. S., et al., 2005, *Natur*, 437, 855
 Woosley S. E., 1993, *ApJ*, 405, 273
 Woosley S. E., Bloom J. S., 2006, *ARA&A*, 44, 507
 Zhang B.-B., et al., 2018, *NatCo*, 9, 447
 Zhang B., Mészáros P., 2001, *ApJ*, 552, L35
 Zhang B., Yan H., 2011, *ApJ*, 726, 90
 Zhang B., et al., 2009, *ApJ*, 703, 1696
 Zhang D., Dai Z. G., 2009, *ApJ*, 703, 461
 Zhang D., Dai Z. G., 2008, *ApJ*, 683, 329

Table 1. The spectral fitting parameters for our sample.

Trigger ID	Components	Model	T_d^a (s)	E_p^b (keV)	α^c	S_γ^d (erg cm ⁻²)	F_p^e (erg cm ⁻² s ⁻¹)	(χ^2 /dof)
bn080807993	Spike	CPL	1.92	515±162	0.73±0.12	(3.55±1.49)e-6	(1.55±1.07)e-5	234/240
	EE	CPL	18.30	453±387	1.16±0.19	(3.72±3.32)e-6	(3.25±0.40)e-7	183/241
bn081110601	Spike	CPL	1.12	507±67	0.75±0.06	(5.89±0.71)e-6	(6.95±0.07)e-6	256/237
	EE	CPL	11.68	170±49	0.88±0.15	(3.01±1.13)e-6	(1.37±0.28)e-7	246/239
bn081129161	Spike	CPL	2.45	320±49	0.82±0.07	(5.12±0.70)e-6	(3.81±0.28)e-6	242/237
	EE	CPL	10.55	267±69	1.03±0.11	(5.92±1.47)e-6	(6.47±4.56)e-7	254/237
bn081215784	Spike	Band	3.72	487±32	-0.53±0.03	(5.30±0.34)e-5	(1.06±0.09)e-4	266/235
	EE	CPL	6.77	300±12	0.77±0.02	(3.31±0.08)e-5	(4.24±0.56)e-5	266/235
bn090720710	Spike	CPL	0.42	535±73	0.37±0.08	(5.11±0.96)e-6	(1.53±1.00)e-5	250/240
	EE	CPL	6.81	520±131	0.87±0.09	(7.02±1.64)e-6	(5.68±3.18)e-6	263/240
bn090831317	Spike	CPL	0.55	339±141	1.10±0.16	(7.92±3.90)e-7	(8.92±4.26)e-6	253/240
	EE	CPL	42.20	1037±584	1.51±0.07	(1.72±0.57)e-5	(2.35±0.05)e-6	194/240
bn090929190	Spike	CPL	1.84	296±30	0.32±0.07	(7.70±0.98)e-6	(1.83±0.03)e-5	225/239
	EE	CPL	8.15	262±92	0.70±0.18	(3.22±1.85)e-6	(8.51±0.74)e-6	229/239
bn091127976	Spike	CPL	2.26	242±16	1.36±0.03	(1.16±0.03)e-5	(8.15±1.70)e-6	260/238
	EE	CPL	12.97	62±8	1.75±0.07	(6.43±0.33)e-6	(2.27±1.87)e-6	268/238
bn100829876	Spike	CPL	2.83	175±11	0.68±0.04	(1.26±0.06)e-5	(2.18±0.55)e-5	222/238
	EE	CPL	10.61	84±22	1.14±0.15	(2.84±0.74)e-6	(1.53±0.20)e-6	262/239
bn110824009	Spike	CPL	1.30	1243±132	0.68±0.04	(1.83±0.20)e-5	(8.41±4.92)e-6	243/238
	EE	CPL	17.20	432±162	1.02±0.11	(7.93±2.88)e-6	(5.02±0.45)e-6	223/239
bn111012811	Spike	CPL	1.07	124±18	0.48±0.10	(2.21±0.39)e-6	(3.93±0.13)e-6	288/237
	EE	CPL	5.33	146±74	0.99±0.22	(1.34±0.83)e-6	(2.03±0.20)e-6	192/239
bn120119229	Spike	CPL	1.40	727±212	0.58±0.13	(4.09±1.78)e-6	(3.97±0.44)e-6	251/239
	EE	CPL	17.36	666±189	0.51±0.14	(1.67±0.81)e-5	(2.32±0.03)e-6	200/239
bn120304248	Spike	CPL	1.31	951±96	0.48±0.05	(1.58±0.20)e-5	(3.53±1.36)e-5	271/239
	EE	CPL	3.94	804±118	0.62±0.06	(1.64±0.26)e-5	(7.75±1.66)e-6	275/239
bn120605453	Spike	CPL	4.75	769±332	1.26±0.08	(4.46±1.22)e-6	(2.25±0.14)e-6	266/235
	EE	CPL	15.48	91±59	1.46±0.32	(1.32±1.10)e-6	(1.50±0.21)e-7	245/237
bn130628531	Spike	CPL	4.65	283±46	1.09±0.06	(7.18±0.74)e-6	(2.51±0.10)e-6	243/239
	EE	CPL	11.56	83±46	1.49±0.28	(1.34±0.95)e-6	(2.40±0.21)e-7	238/239
bn131108862	Spike	CPL	0.70	568±90	0.82±0.06	(5.19±0.74)e-6	(2.03±1.07)e-5	271/241
	EE	CPL	18.76	384±32	0.96±0.03	(3.39±0.16)e-5	(3.60±0.18)e-6	242/241
bn140308710	Spike	CPL	3.20	197±28	0.60±0.09	(3.83±0.64)e-6	(6.36±3.12)e-6	263/242
	EE	CPL	13.50	164±45	1.19±0.12	(3.55±0.82)e-6	(2.16±0.16)e-6	276/242
bn141229492	Spike	CPL	2.50	226±30	0.38±0.10	(4.43±0.86)e-6	(4.62±0.91)e-6	299/237
	EE	CPL	10.17	80±29	0.88±0.26	(1.20±0.79)e-6	(3.12±2.26)e-7	243/237
bn150127398	Spike	CPL	1.68	866±223	0.51±0.12	(8.20±3.14)e-6	(2.47±0.03)e-5	249/240
	EE	CPL	7.80	778±236	0.76±0.10	(1.09±0.36)e-5	(3.55±1.84)e-6	224/240
bn150510139	Spike	CPL	1.58	765±43	0.54±0.03	(3.37±0.17)e-5	(2.67±0.79)e-5	251/239
	EE	CPL	36.62	744±129	0.75±0.06	(9.76±1.68)e-5	(1.05±0.01)e-5	222/239
bn150702998	Spike	CPL	4.46	951±211	0.64±0.09	(1.11±0.30)e-5	(1.51±1.27)e-5	268/239
	EE	CPL	18.90	865±240	0.86±0.09	(1.84±0.53)e-5	(7.46±0.33)e-6	231/239
bn160721806	Spike	CPL	0.40	288±109	0.30±0.32	(9.83±5.81)e-7	(5.56±0.39)e-6	241/238
	EE	CPL	8.49	163±61	0.88±0.23	(2.55±1.92)e-6	(4.24±0.59)e-7	215/238
bn161218356	Spike	CPL	4.35	185±9	0.73±0.03	(1.96±0.06)e-5	(2.43±0.50)e-5	258/239
	EE	CPL	26.76	146±4	0.46±0.02	(6.60±0.13)e-5	(1.46±0.97)e-5	226/239
bn170115743	Spike	CPL	2.51	1337±65	0.55±0.03	(5.23±0.26)e-5	(5.98±2.63)e-5	247/239
	EE	CPL	36.28	1272±142	0.97±0.03	(8.26±0.70)e-5	(1.32±0.01)e-5	246/239
bn170527480	Spike	CPL	2.31	624±61	0.71±0.04	(1.41±0.11)e-5	(2.08±0.81)e-5	273/239
	EE	CPL	60.48	577±69	0.79±0.06	(1.10±0.11)e-4	(7.50±0.99)e-6	211/239
bn170626401	Spike	CPL	3.42	88±5	0.59±0.05	(6.77±0.27)e-6	(5.54±2.58)e-6	246/239
	EE	CPL	11.24	81±7	0.92±0.06	(7.28±0.40)e-6	(2.59±0.08)e-6	252/241

^a Durations of the hard spike and EE for our sample.^b Peak energy of CPL or Band model fits of the hard spike and EE.^c The low-energy photon index of CPL or Band model fits for the hard spike and EE.^d Energy fluence of the hard spike and EE.^e Peak flux of CPL or Band model fits of the hard spike and EE.

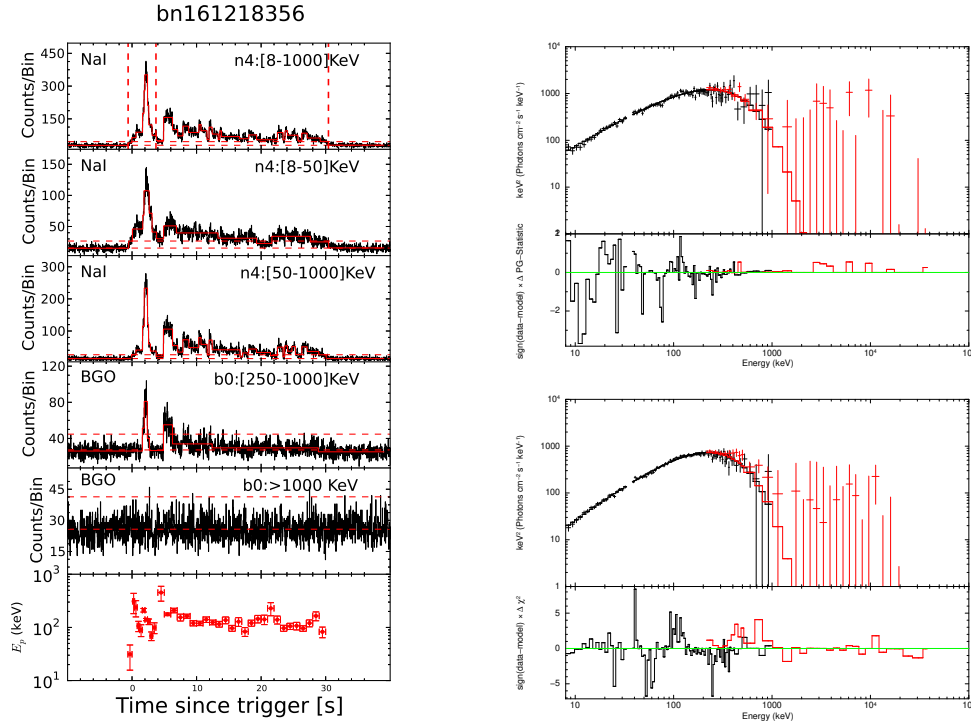


Figure 1. An example of GRB 161218 lightcurve and spectrum, together with our Bayesian block analysis (red blocks in the left panel), time-integrated spectral fits for the hard spike and subsequent EE (solid line in the right panel), and E_p evolution of the prompt emission phase. The dashed horizontal lines in the left panel are a 3σ signal over background emission. The dashed vertical lines are the beginning, separation, and end of the hard spike and EE, respectively.

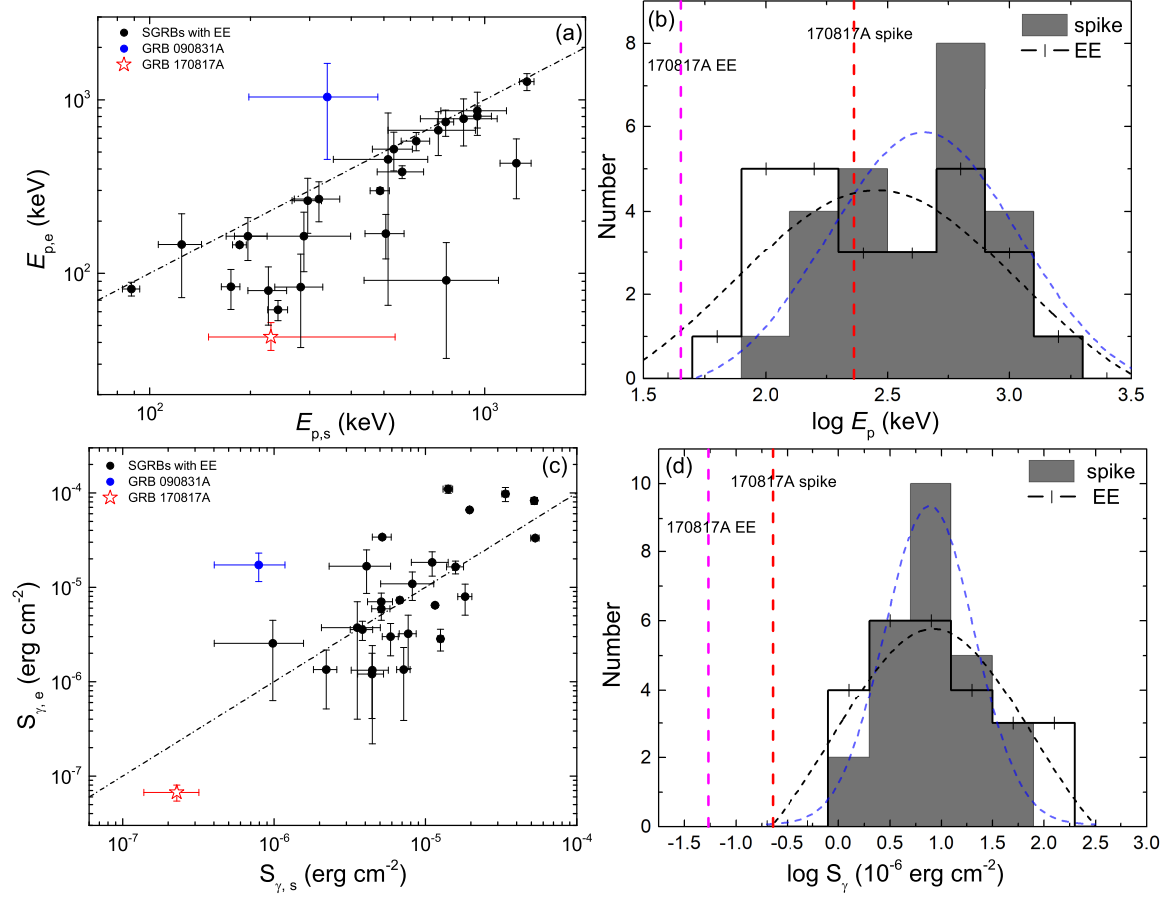


Figure 2. $E_{p,s} - E_{p,e}$ (a) and $S_{\gamma,s} - S_{\gamma,e}$ (c) correlations for the short GRBs with EE in our sample. The black dashed-dotted lines correspond to $E_{p,s} = E_{p,e}$ in (a) and $S_{\gamma,s} = S_{\gamma,e}$ in (c), respectively. The opened-red star is the GRB 170817A. (b) and (d) show the distributions of peak energy and fluence for the hard spike and EE in our sample. Best-fit Gaussian profiles are denoted in black and blue dashed lines, respectively. The red and magenta dashed vertical lines correspond to the hard spike and EE of GRB 170817A, respectively.

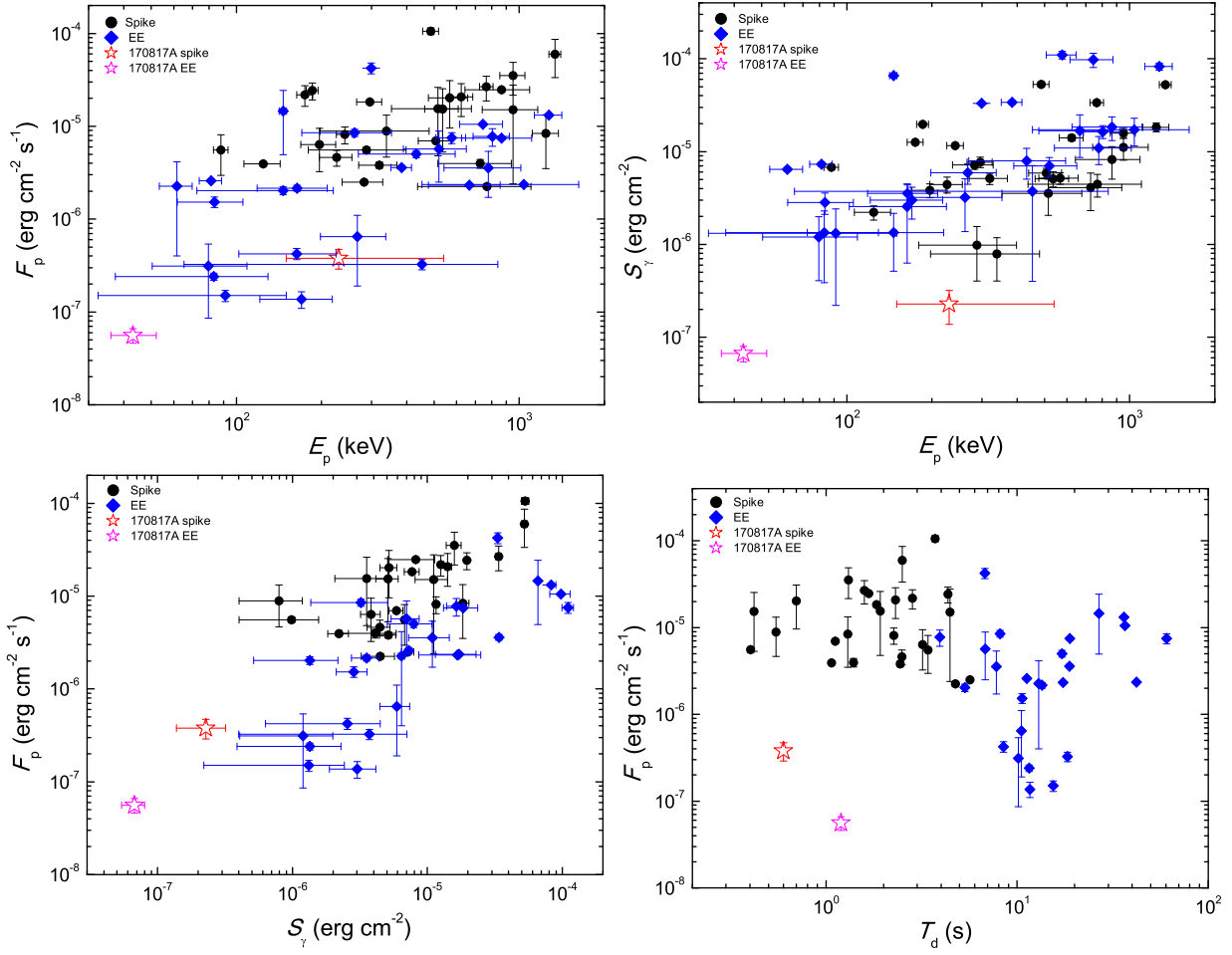


Figure 3. $E_p - F_p$, $E_p - S_\gamma$, $S_\gamma - F_p$, and $F_p - T_d$ correlations of hard spike and EE in our sample. The red and magenta opened stars correspond to the spike and EE of GRB 170817A, respectively.

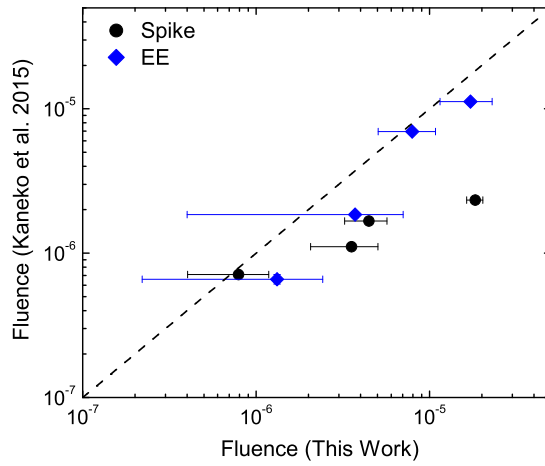


Figure 4. Comparison of the estimated fluence in EE and hard spike with Kaneko et al. (2015) for the four overlapping GRBs. The dashed line is the equivalent fluence between our calculation and Kaneko et al. (2015).

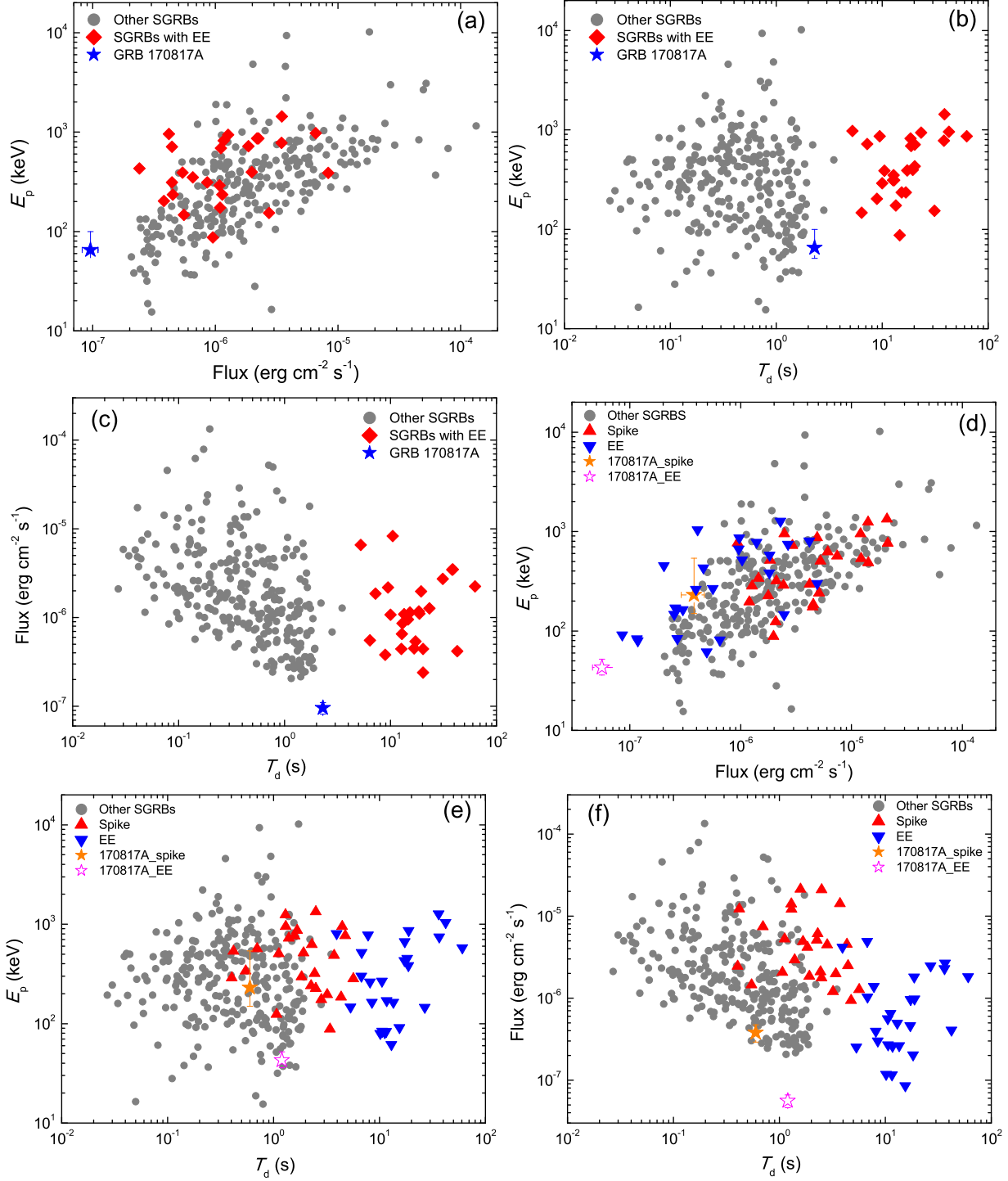


Figure 5. (a)-(c): E_p – Flux, E_p – T_d , and Flux – T_d diagrams for short GRBs with EE in our sample (black diamonds) and other short GRBs (gray dots; taken from Lu et al. 2017). (d)-(f): E_p – Flux, E_p – T_d , and Flux – T_d diagrams for hard spike (black triangles), EE (blue triangles), and other short GRBs (gray dots). The hard spike and EE of GRB 170817A are marked with opened red and magenta stars, respectively.

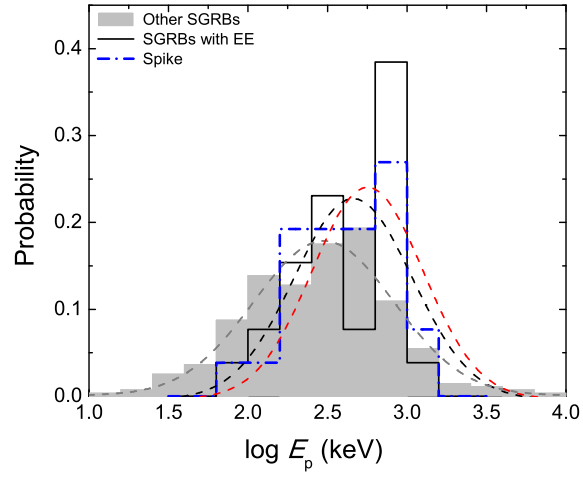


Figure 6. Distributions of E_p for the time-integrated spectra of other short GRBs (gray column), short GRBs with EE (black solid line), as well as the sample of hard spikes of short GRBs with EE (blue dashed-dotted line). The best-fit Gaussian profiles correspond to the respective colors, respectively.